

## Article

# Study on Electrical Characteristics Analysis and Electrical Circuit Model Design of Vanadium Redox Flow Battery Systems Based on Current and Flow Rate Conditions

Seongjun Lee <sup>1</sup>, Hyeonhong Jung <sup>2</sup> and Yoon-Gyung Sung <sup>1,\*</sup> 

<sup>1</sup> Department of Mechanical Engineering, Chosun University, Gwangju 61452, Republic of Korea; lsj@chosun.ac.kr

<sup>2</sup> Mobase Electronics, Suwon 16648, Republic of Korea; gusghd0707@naver.com

\* Correspondence: sungyg@chosun.ac.kr; Tel.: +82-62-230-7181

**Abstract:** Recent research has focused on vanadium redox flow batteries (VRFBs) to address the short lifetimes and fire risks associated with lithium battery systems. While VRFBs offer advantages in safety, they suffer from low energy density and efficiency compared with lithium batteries. To improve VRFB performance, studies are exploring improvements in materials such as anodes, cathodes, and separators and optimizing operations by controlling electrolyte flow rates. However, the impact of current magnitude on VRFB efficiency has been less studied, with few analyses addressing both current and flow rate effects. This research proposes an experimental procedure to evaluate charge/discharge efficiency, energy efficiency, and system efficiency across varying current magnitudes and electrolyte flow rates, using a 40 W VRFB stack composed of four 10 W cells in series. In addition, we introduce a design method for an electrical equivalent circuit model that simulates the VRFB stack, reflecting experimental findings. The model's accuracy was validated by comparing it with data from 11 full charge/full discharge cycle tests, which varied current and electrolyte amounts.

**Keywords:** vanadium redox flow battery (VRFB); energy storage system (ESS); efficiency; electrical circuit model (ECM); flow rate; electrolyte; current magnitude; charge/discharge cycle test



**Citation:** Lee, S.; Jung, H.; Sung, Y.-G. Study on Electrical Characteristics Analysis and Electrical Circuit Model Design of Vanadium Redox Flow Battery Systems Based on Current and Flow Rate Conditions. *Energies* **2024**, *17*, 5841. <https://doi.org/10.3390/en17235841>

Academic Editor: King Jet Tseng

Received: 25 October 2024

Revised: 17 November 2024

Accepted: 20 November 2024

Published: 21 November 2024



**Copyright:** © 2024 by the authors. Licensee MDPI, Basel, Switzerland. This article is an open access article distributed under the terms and conditions of the Creative Commons Attribution (CC BY) license (<https://creativecommons.org/licenses/by/4.0/>).

## 1. Introduction

Because the use of fossil fuels, such as oil and coal, causes global warming, environmental pollution, and resource depletion, industries that use eco-friendly renewable energy sources, such as solar and wind power, are attracting attention to solve these problems. However, renewable energy power generation systems have intermittent characteristics that depend on environmental conditions such as solar irradiance and wind speed. Energy storage systems (ESSs) that overcome these renewable energy problems and enable stable and efficient power and energy management are growing steadily [1,2]. The electrical energy sources used in ESSs include lead–acid batteries, lithium batteries, sodium–sulfur batteries, redox flow batteries, supercapacitors, and compressed air. Table 1 lists the energy densities, energy efficiencies and lifetimes of the electrical energy sources in an ESS [2]. Currently, lithium-ion batteries with high energy densities and efficiencies are widely used in ESSs to maximize energy efficiency [2,3].

However, energy storage devices that use lithium-ion batteries have several problems. As can be seen from the fire accidents of large-capacity batteries applied to electric vehicles, energy storage devices composed of lithium-ion batteries using flammable nonaqueous organic solvents face the problem of fire when thermal runaway occurs because of internal short circuits [4–6]. In particular, energy storage devices manufactured by combining a large number of lithium-ion battery cells in series and in parallel have a higher possibility of fire occurrence if the maximum and minimum voltages of the applied battery cells cannot be managed and if the failure status cannot be accurately predicted to maintain the cells or

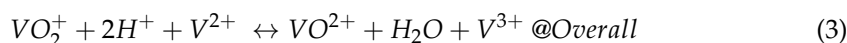
modules. Therefore, when lithium-ion batteries are used in large-capacity energy storage applications, considerable effort must be made to prevent fires and prevent them from spreading. Accordingly, to estimate the battery status, recent research on fault detection using gas sensors and force sensors, as well as voltage and temperature measurements, has been conducted [7]. In addition, research is being conducted on estimating SOC and temperature by training an artificial intelligence model using measurement signals using non-destructive techniques such as ultrasonic sensors [8]. In addition, lithium-ion batteries cause environmental pollution during disposal after their lifespan ends [9]. To solve these problems, research is being conducted to improve lithium-ion battery deterioration diagnosis and reuse. However, this increases the operational complexity and cost of the system [10,11].

**Table 1.** Energy and efficiency of energy storage system [2].

	Lead–Acid	Lithium-Ion	NaS	VRFB	Super Capacitors	CAES *
Energy Density (Wh/L)	50–80	200–500	150–250	16–33	2–10	3–6
Energy Efficiency (%)	70–90	85–95	80–90	70–85	90	45–60
Lifetime (cycles)	500–800	2000–3000	4000–40,000	1500–15,000	50,000	>10,000

\* CAES: Compressed Air Energy Storage.

Therefore, research is being conducted on battery systems that can replace lithium-ion batteries in ESSs, and the Vanadium Redox Flow Battery (VRFB), which uses an aqueous solvent with a longer lifespan than lithium batteries, is being studied extensively [12–19]. In a VRFB system, positive and negative electrolytes are stored in two electrolyte tanks, and the flow is supplied in parallel to the series-connected cells inside the stack through a pump. The transferred electrolyte undergoes an oxidation/reduction reaction at the electrode, ions move to the ion exchange membrane of the Nafion material, and energy is stored in the electrolyte. The oxidation/reduction reaction of the VRFB is shown in Figure 1 and can be expressed by the anode, cathode, and overall electrochemical reaction formulas in Equations (1) to (3). The ionic reaction of the vanadium electrolyte is that when charging, the  $V^{3+}$  ions at the negative electrode are reduced to  $V^{2+}$  ions, and the  $V^{4+}$  ions at the positive electrode are oxidized to  $V^{5+}$  ions. During the discharging process, the  $V^{5+}$  ions at the positive electrode are oxidized to  $V^{4+}$  ions, and the  $V^{2+}$  ions at the negative electrode are oxidized to  $V^{3+}$  ions, thereby performing charging and discharging.



The output of the VRFB was determined by the area of the electrode, and the voltage of the system was determined by the number of cells connected in series. Unlike lithium-ion batteries, which increase capacity by connecting cells with the same characteristics in parallel, the VRFB is determined by the amount of electrolyte stored in the tank. Therefore, VRFBs have the advantages of increasing capacity and being more flexible in mechanical design than existing cylindrical, square, and pouch-shaped lithium-ion battery packaging designs [13]. However, VRFBs have a lower energy density and efficiency than lithium-ion batteries, and to achieve the same energy capacity as an ESS using lithium-ion batteries, the VRFB system requires a larger installation area and initial investment costs.

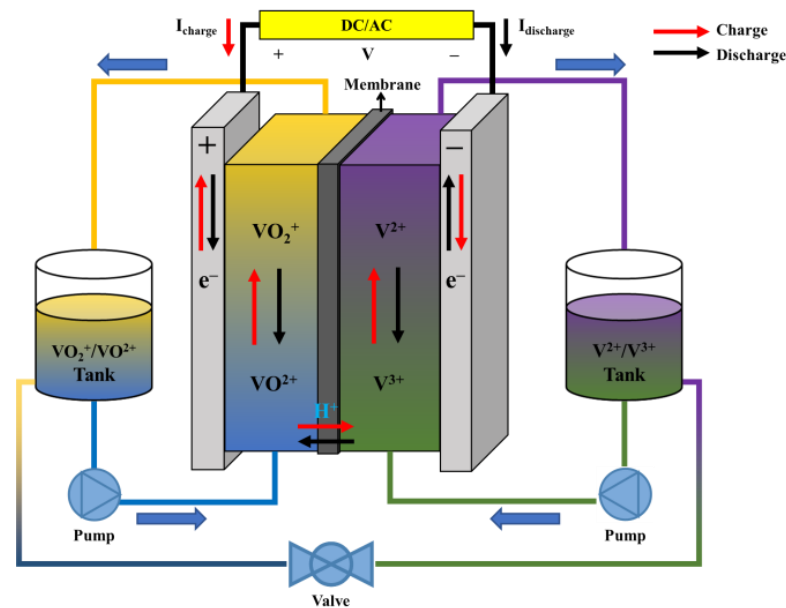


**Figure 1.** Diagram of VRFB energy storage system [19].

In order to overcome the disadvantages of low energy density and efficiency of VRFBs, research is being conducted on the materials of vanadium electrolytes and felt electrodes, as well as on membranes that affect crossover by ion selectivity [20,21]. To this end, VRFBs require an analysis of system efficiency, including charge/discharge Coulomb efficiency, energy efficiency, and pump loss through charge/discharge experiments according to current and flow conditions. In addition, to analyze the electrical characteristics of the VRFB system according to the flow rate and current conditions, electrical equivalent circuit modeling of the VRFB and parameter analysis are required. Unlike the electrical ECM model of a lithium battery, the VRFB must be modeled such that the shunt current loss that occurs as the electrolyte is connected in parallel to the cells inside the stack and a capacity change depending on the amount of electrolyte is possible.

Previous studies on improving the VRFB efficiency are as follows. Kim presented the discharge characteristics of a 1 kW/1 kWh VRFB using mixed-acid electrolytes and the advantages of using electrolytes [22]. The study presented the VRFB discharge characteristics and efficiency results according to the current and flow rate conditions but did not present the parameter analysis results of the electrical equivalent circuit model. Karrech analyzed charge and discharge experimental results according to variable flow rate conditions and presented a flow rate control method for optimal efficiency [23]. However, the shunt current loss was not considered because it was conducted on a single cell and its characteristics depended on the current size. Ma. X conducted a study on the optimal flow condition at the VRFB stack level but did not mention the influence of the current size for optimal efficiency control in detail [24]. Thus, to improve the efficiency of the VRFB battery system, it is necessary to comprehensively consider the influence of the shunt current and analyze the VRFB system characteristics on the charge/discharge current and flow conditions during operation.

Previous studies on the design of electrical equivalent circuit modeling are as follows: Fornaro presented the same electrical equivalent circuit model used in this study and estimated its parameters using recursive least squares (RLS) [25]. However, the study presented parameter estimation results from short-term simulations that did not consider the influence of the shunt current loss. However, in a series-connected stack system, the influence of shunt current should be considered. Yu Zhang also presented the same electrical equivalent circuit model considering the shunt resistance and showed that the stack could be well simulated with the estimated parameters using RLS [26]. This study considered the influence of the shunt current and flow rate; however, because the simulation

results were for a short period, a method to simulate the change in electrolyte volume owing to crossover was not presented.

Therefore, in this study, we propose an experimental method that can analyze the charge/discharge Coulombic efficiency, energy efficiency, and system efficiency according to the current size and electrolyte flow rate conditions and present the results of the system efficiency analysis for a 40 W VRFB stack composed of four 10 W cells in series. In addition, we systematically present an electrical equivalent circuit model that can simulate the VRFB stack and an experimental procedure and analysis method for estimating its parameters.

## 2. Experimental Setup and Characteristic Experimental Profile Design of VRFB

### 2.1. VRFB Experimental Setup

The VRFB stack used in this study has the configuration shown in Figure 2. The stack was manufactured with a structure in which a pair of bipolar plates, flow frames, electrodes, and membranes formed a cell, and four pairs were connected in series. The VRFB cell/stack used in this study has four input/output ports on one endplate for electrolyte transport. The four ports comprise two inlet ports through which the electrolyte is transferred to the cells inside the stack and two outlet ports through which the electrolyte that has undergone oxidation/reduction reactions inside the cell is transferred to the outside. The felt and bipolar plate are made of graphite for electrical conductivity, and the ion separation membrane is NR212, with a thickness of 50  $\mu\text{m}$  [27].

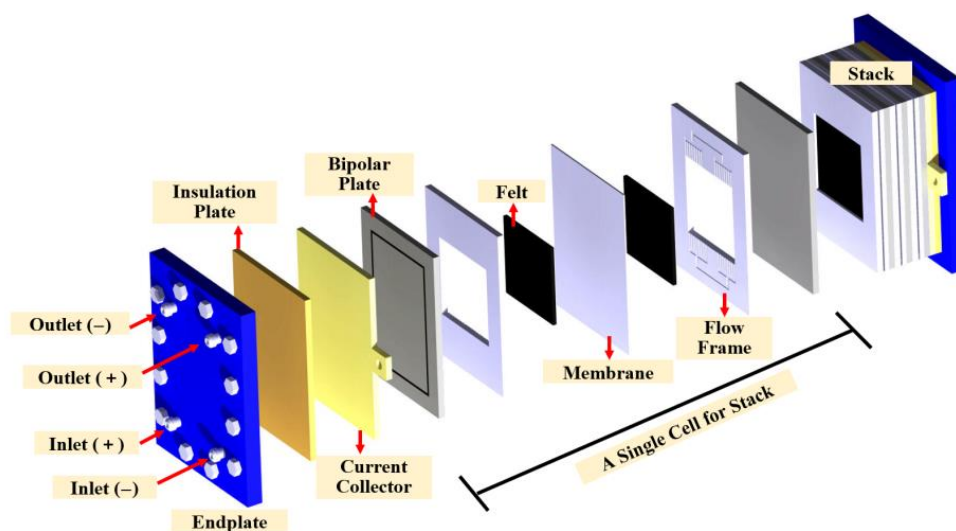
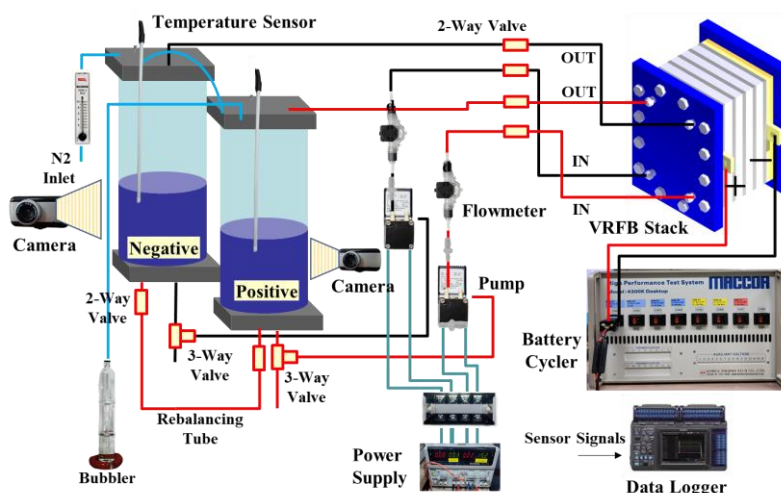
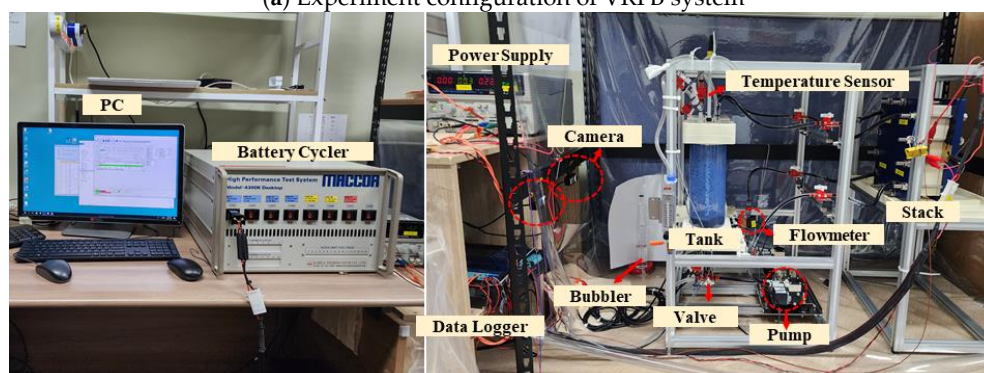


Figure 2. VRFB stack configuration diagram.

The charge/discharge experimental configuration of a 40 W VRFB stack with four 10 W cells connected in series used in this study is shown in Figure 3a, and a diagram of the actual constructed system is shown in Figure 3b. The VRFB stack system had two tanks for storing the electrolyte consisting of 1.6 M  $\text{V}^{3.5+}$  / 2 M  $\text{H}_2\text{SO}_4$ , a diaphragm pump, and a flowmeter to measure the flow rate. Additionally, both electrolyte tanks were connected to a flow tube to balance the electrolyte in case of electrolyte imbalance due to crossover. The volume of the electrolyte was measured every 5 min during the experiment using cameras applied to positive and negative electrolyte tanks. The VRFB was charged and discharged using a battery cyler, and the measured stack voltage, current, temperature, flow rate, voltage, and current consumed by the pump were stored in a data logger at a sampling time of 100 ms. Table 2 lists the main specifications of the VRFB stack and the peripheral devices used in the experiment described above.



(a) Experiment configuration of VRFB system



(b) Experimental setup

**Figure 3.** VRFB stack system configuration; (a) experiment configuration of VRFB system, (b) experimental setup.

**Table 2.** Specification for VRFB stack system.

40 W VRFB Stack System		
VRFB Stack	Electrode Area	100 cm <sup>2</sup> (10 × 10)
	Electrolyte	1.6 M V <sup>3.5+</sup> / 2 M H <sub>2</sub> SO <sub>4</sub>
	Membrane	Nafion-212
	Electric Collector	Brass
	Electrode	Carbon Felt
Battery Cycler	Maccor 4300 K	
Electrolyte Volume	210 mL (±5 mL)	
Pump	KNE, NF60	
Flowmeter	Omega, FTB-312	
Thermal Sensor	Teflon PT100/Thermocouple (T-type)	

## 2.2. Design of Experimental Procedure for Electrical Characteristics of VRFB

It is difficult to experiment with VRFBs under the same capacity (electrolyte volume) conditions because of electrolyte crossover when the experiments are conducted over a long period. This is because the VRFB operating point changes, making it challenging to analyze the characteristics under various experimental conditions. The crossover of the electrolyte can be reduced through improvements such as ion concentration control, changes in membrane thickness, and material modifications [28,29]. However, since this

paper analyzes the electrical characteristics of an already-constructed VRFB system, the experiments were conducted following the procedure shown in Figure 4, minimizing the impact of crossover.

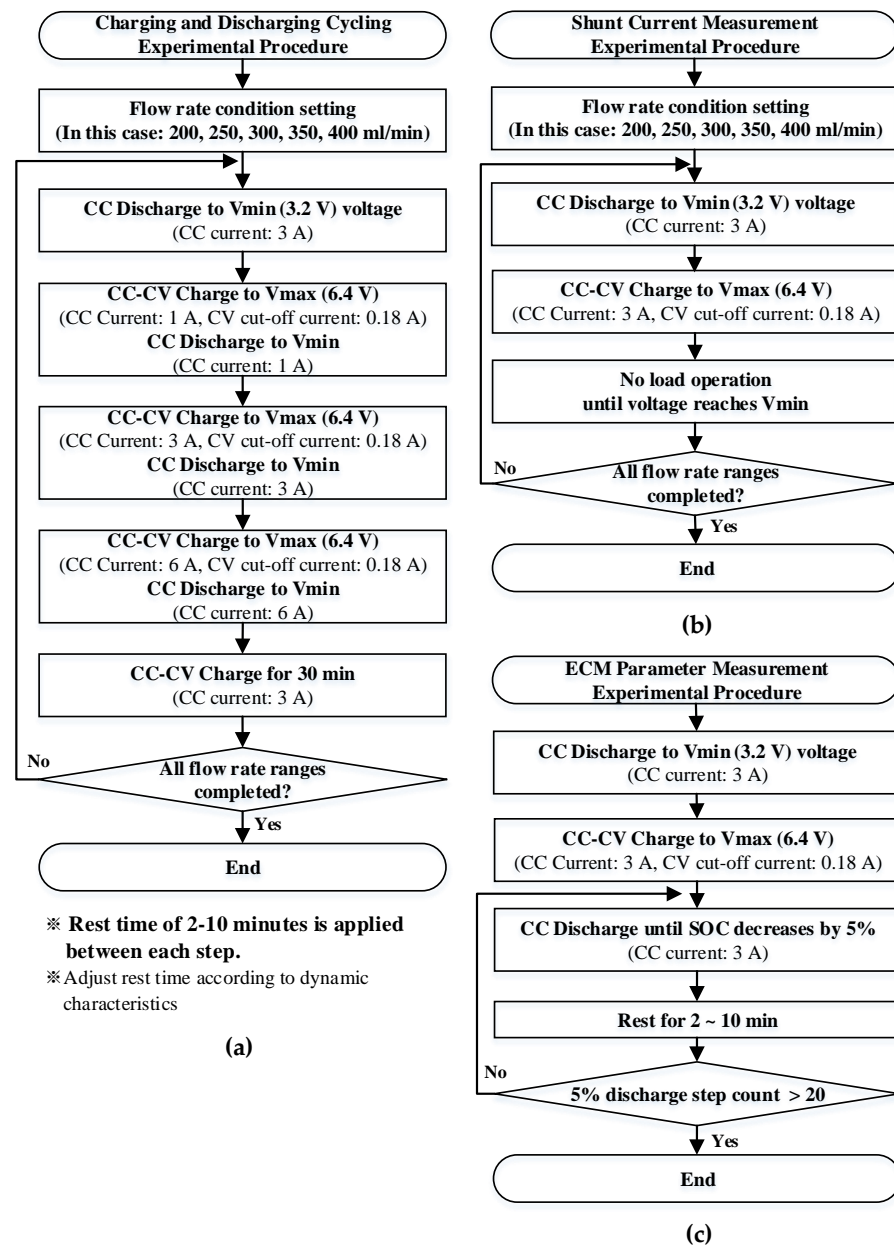


**Figure 4.** VRFB experimental profile; (a) charging and discharging experimental procedure, (b) shunt current measurement experimental procedure, and (c) ECM parameter measurement experimental procedure.

The experimental procedure for analyzing the Coulombic, energy, and system efficiencies of the VRFB stack is shown in Figure 4a. First, the charging and discharging cycles were performed continuously under current conditions of 1, 3, and 6 A (10, 30, and 60 mA/cm<sup>2</sup>) with a fixed flow rate. The charging and discharging capacities were measured according to the current magnitude, and the Coulomb efficiency was analyzed. Subsequently, the same experiment was carried out by changing the flow rate condition so that the influence of each flow rate could be analyzed. In this study, tests were performed in the range of 200–400 mL/min at intervals of 50 mL/min intervals. The VRFB stack used in this experiment was charged by the Constant Charge–Constant Voltage (CC-CV) method with a

full charge voltage of 6.4 V (1.6 V per cell) and a cut-off current of 0.18 A for terminating CV charge, and the full discharge voltage is 3.2 V (0.8 V per cell) and discharged with CC current.

The VRFB stack has a shunt current loss owing to internal self-discharge because the electrolyte is connected in parallel to each cell. The experimental procedure for extracting the shunt current and resistance parameters is shown in Figure 4b. First, the pump was driven under conditions of no load current while the battery stack was fully charged at a fixed flow rate. In this case, the voltage of the battery gradually decreased owing to the shunt current, and the experiment was conducted until the battery was fully discharged (cut-off voltage of 3.2 V). The shunt current was obtained by dividing the capacity measured when fully charged by the time required for complete discharge. Subsequently, the same experiment was conducted by changing the flow rate conditions, and the shunt current loss was analyzed according to the flow rate.

The experimental profile for measuring the open-circuit voltage of the VRFB and parameters of the equivalent electrical circuit are shown in Figure 4c. After the battery was fully charged, a pulse current was applied to discharge the SOC to 5%, followed by a rest period. This pulse current, including the rest time, was repeatedly applied until the stack voltage reached the full discharge voltage. Through this experiment, the parameters  $R_i$ ,  $R_d$ , and  $C_d$  of the electrical equivalent circuit were obtained from the voltage response characteristics when a pulsed current was applied, and the open-circuit voltage (OCV) at a specific SOC was obtained for each rest period.

### 3. Efficiency Analysis and ECM Modeling of VRFB

In this section, we present the energy efficiency analysis results of the VRFB system according to the current magnitude and flow rate changes using the voltage/current and pump power consumption data measured during the charge/discharge test of the VRFB, using the test procedure shown in Figure 4. The Coulomb, voltage, energy, and system efficiency of the VRFB were calculated using Equations (4)–(7). Equation (4) represents the Coulomb efficiency, which is defined as the ratio of the charge capacity to the discharge capacity. Voltage efficiency is an index for analyzing the influence of the polarization voltage or overvoltage on the battery voltage and is defined in Equation (5). The energy efficiency is expressed as the ratio of the discharge energy to the charge energy, as shown in Equation (6). The system efficiency was calculated using Equation (7), including the energy consumed by the pump used to drive the VRFB stack and the energy of the VRFB stack itself during battery charging and discharging.

$$\text{Coulombic Efficiency}(\%) = \frac{\text{Discharge Capacity}(\text{Ah})}{\text{Charge Capacity}(\text{Ah})} = \frac{\int I_{Dchg}(t)dt}{\int I_{Chg}(t)dt} \times 100 \quad (4)$$

$$\text{Voltage Efficiency}(\%) = \frac{\int V_{Dchg}(t)dt}{\int V_{Chg}(t)dt} \times 100 \quad (5)$$

$$\text{Energy Efficiency}(\%) = \frac{\int V_{Dchg}(t) \times I_{Dchg}(t)dt}{\int V_{Chg}(t) \times I_{Chg}(t)dt} \times 100 \quad (6)$$

$$\text{System Efficiency}(\%) = \frac{\int (V_{Dchg}(t) \times |I_{Dchg}(t)| - P_{pump})dt}{\int (V_{Chg}(t) \times |I_{Chg}(t)| + P_{pump})dt} \times 100 \quad (7)$$

#### 3.1. Efficiency Analysis of VRFB According to Current and Flow Rate

Figure 5 shows the voltage and current waveforms, electrolyte volume changes, and pump power consumption results when the VRFB stack was charged and discharged under 100% depth of discharge (DoD) conditions; the current profile is shown in Figure 4a when the electrolyte flow rate was 250 mL/min. As can be seen in (a) voltage and (b) current in Figure 5, as the charge and discharge currents increase, the voltage decrease size increases,

and the CV charge arrival time becomes faster, showing the characteristic of a longer charging time. Figure 5c shows the volume of the negative electrolyte measured during the test. The volume of the negative electrolyte decreases when the state of charge is low (as the voltage decreases) and increases when the state of charge increases (as the voltage increases). And the average volume of the electrolyte during the experimental profile was 174 mL. The pump power required to transport the electrolyte in the VRFB during the experiment is shown in Figure 5d. The pump consumed an average of 3.27 W of power when operated at a flow rate of 250 mL/min flow rate.

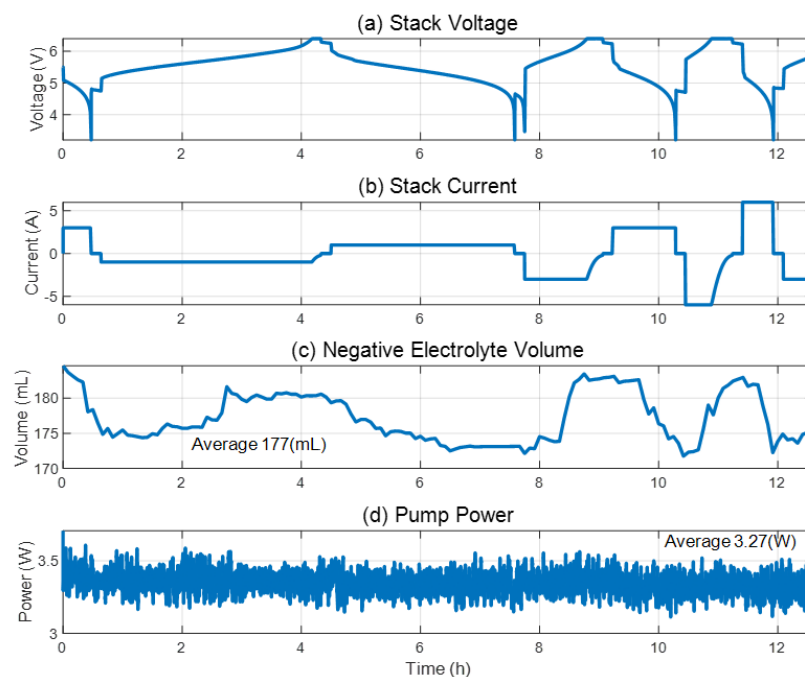


**Figure 5.** Experimental results of VRFB system according to current magnitude at 250 mL/min flow rate: (a) stack voltage; (b) stack current; (c) negative electrolyte volume; (d) pump consumed power.

To analyze the effect of the flow rate conditions on the charge and discharge capacities, experiments were conducted by changing the flow rate conditions under the same conditions as the current profile in Figure 5. The experimental results at the flow rates of 200 mL/min are shown in Figure 6a, 300 mL/min in Figure 6b, 350 mL/min in Figure 6c, and 400 mL/min in Figure 6d, respectively. At this time, as can be seen in the third waveform of the experimental waveforms in Figures 5 and 6, for the negative electrolyte volume, a total of five experiments for characteristic comparison were conducted with similar electrolyte volumes, averaging 174–179 mL. If the electrolyte volume changes significantly as the experiment progresses, it should be maintained by rebalancing before the experiment is conducted. The pump consumes an average power of 3.01, 3.27, 4.58, 6.03, and 7.85 W when controlling the flow rates of 200, 250, 300, 350, and 400 mL/min, respectively.

Figure 7 shows the changes in the charge/discharge capacity, Coulomb efficiency, and voltage efficiency according to the flow rate and current magnitude in the previous cycling experiment. Figure 7a shows that the charge capacity is the largest under a current of 1 A, and the charge capacity decreases as the current increases. It can also be observed that the battery charge capacity decreased as the flow rate increased, even when the current was the same. However, as confirmed from the discharge capacity results in Figure 7b, at currents above 3 A, the same characteristic of decreasing discharge capacity was observed as the current increased. However, when discharging the battery with a constant current of 1 A, the result was smaller than the discharge capacity measured during the 3 A test. This indicates that the VRFB has poor low-current discharge characteristics, owing to the shunt current loss that occurs when the pump is driven, as mentioned in Section 3.2. When a small current is used from the battery, energy transfer takes a long time. Therefore, as the

time at which the pump is operated increases, the energy loss owing to the shunt current also increases, resulting in poor efficiency.

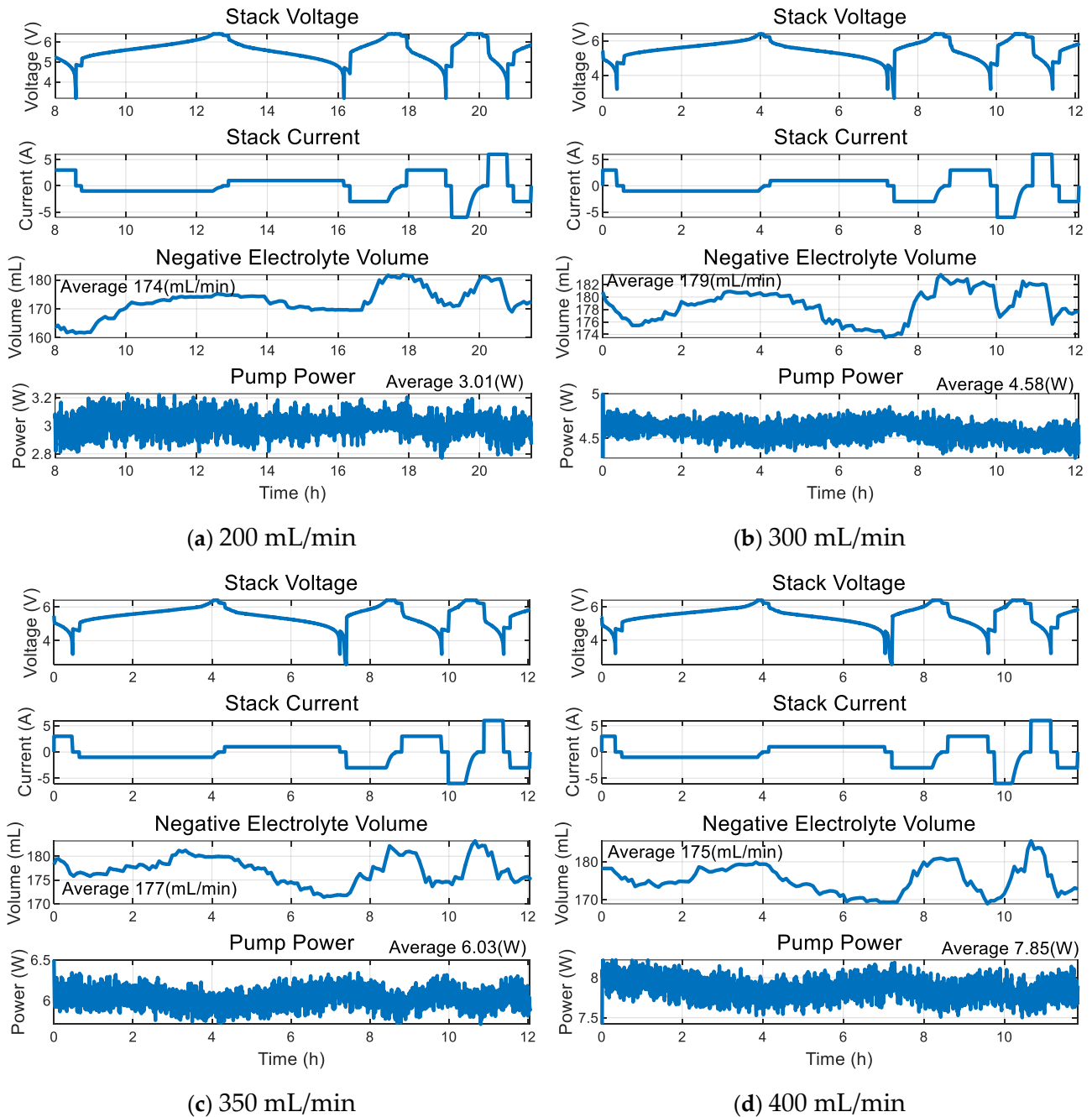


**Figure 6.** Stack voltage, current, cathode electrolyte amount, and pump power consumption of VRFB according to flow conditions: (a) 200 mL/min; (b) 300 mL/min; (c) 350 mL/min; (d) 400 mL/min.

Figure 7c shows the Coulomb efficiency calculated using Equation (4). As mentioned above, when charging/discharging at 1 A under all flow rate conditions, the Coulomb efficiency is 84.9%, which is not good, whereas the results at 3 A and 6 A confirm that the Coulomb efficiency improves to approximately 92.5% as the current increases. Therefore, to increase the usable discharge capacity and improve the Coulomb efficiency, it can be seen that the VRFB system tested in this study should be operated at high current under low-flow rate conditions. In this study, results below 200 mL/min could not be tested due to the limited speed control range of the pump used in the experimental setup. If the flow rate continues to decrease, it is expected that the charge/discharge capacity will decrease

due to insufficient electrolyte supply, and it is judged that appropriate low-flow conditions can be determined based on this. In addition, it should be noted that the results above are from the experimental set environment of this study. In a situation where the VRFB is operated in conjunction with a renewable energy generation system, the generated energy should be transferred to the VRFB and the utility grid as much as possible, so further research on maximum efficiency operation control is required.

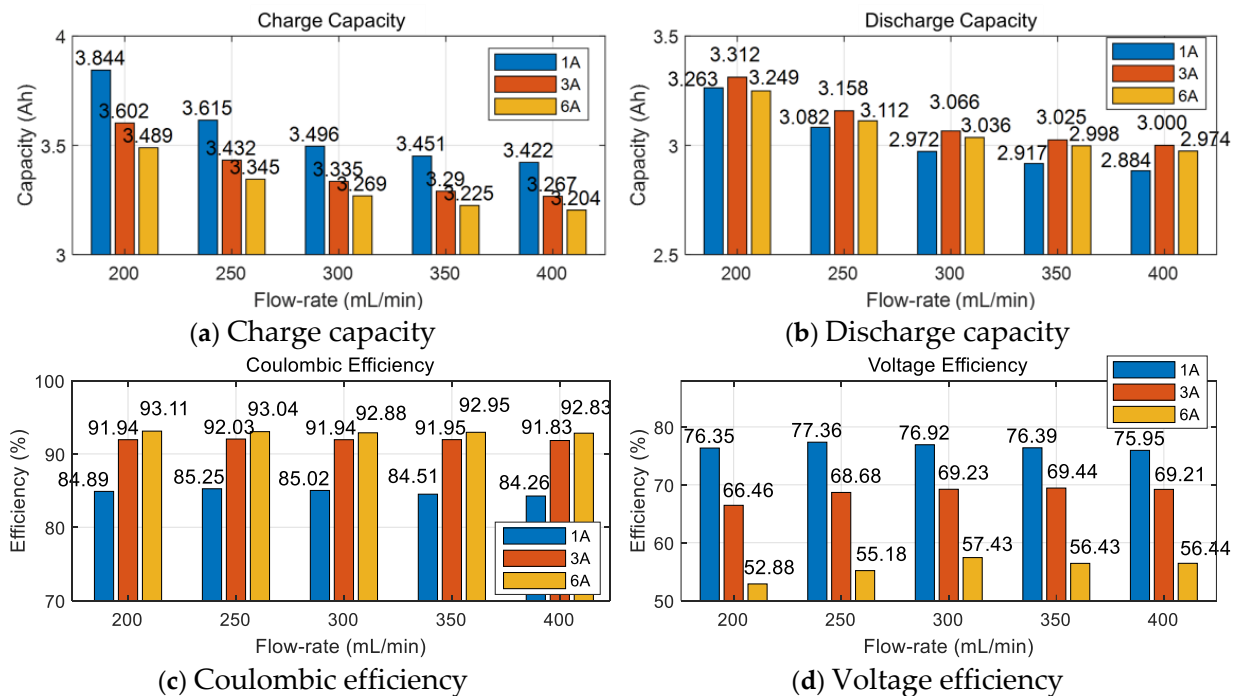


**Figure 7.** VRFB charge/discharge characteristic analysis under different current and flow conditions: (a) charge capacity; (b) discharge capacity; (c) Coulombic efficiency; (d) voltage efficiency.

Figure 7d shows the voltage efficiency calculated by Equation (5). As the current increases, the voltage efficiency deteriorates owing to battery overvoltage. The voltage efficiency does not show a large difference depending on the flow rate change, but it is expected that the efficiency will be somewhat higher overall regardless of the current when operating at a flow rate of 250 mL/min to 300 mL/min. However, the voltage efficiency mentioned above is specific to the context of this study, and the efficiency characteristics may vary when the electrode material is altered or an electrode using a catalyst is used [30].

Figure 8 shows the charge and discharge energies of the characteristic analysis experiment based on the current, flow rate, and energy efficiency calculated using Equation (6). As shown in Figure 8a, the charge energy is the largest when the current is 1 A at a flow rate of 200 mL/min. However, the charged energy can only be transferred to the load side at 17.65 Wh due to a low efficiency of 79.6%. When the battery is charged and discharged at 3 A at 200 mL/min, 79.3% of the charged energy can be transferred, similar to when it is charged and discharged at 1 A.

As shown in Figure 8c, because the energy efficiency decreased as the flow rate increased, it was expected that the energy efficiency could be improved by operating under low-flow conditions. In addition, the VRFB shows that the energy efficiency of the stack itself, which does not consider the loss of peripheral devices such as pumps, is not good, as the voltage efficiency increases as the current increases; thus, it shows that the results can be obtained by operating under low-current conditions to obtain high efficiency. However, because the VRFB has pump loss, the system efficiency, including this, should be analyzed to determine an efficient operation method.

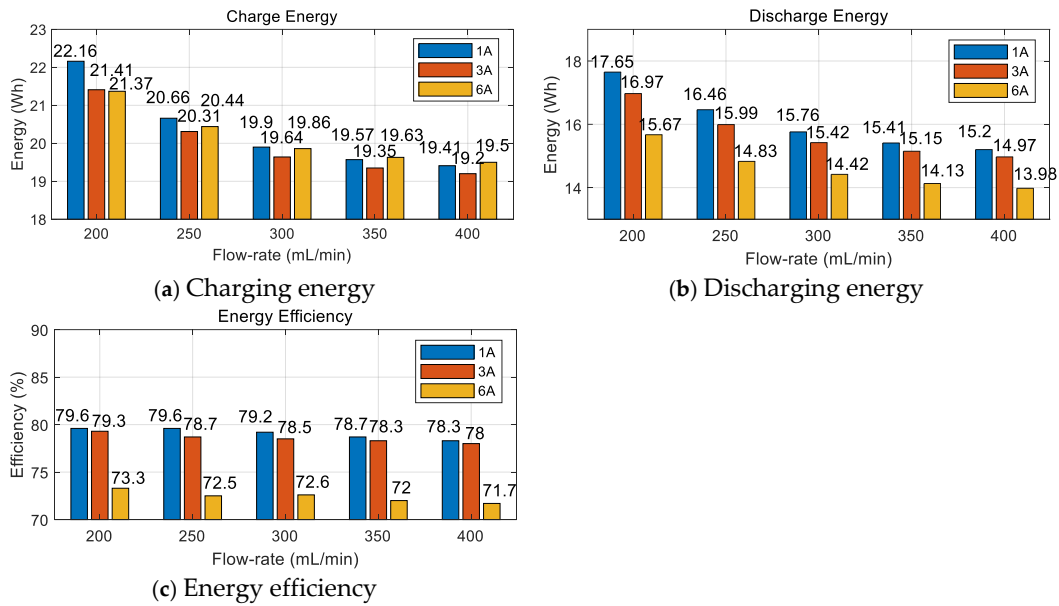


**Figure 8.** VRFB charge/discharge energy and energy efficiency under different current and flow conditions: (a) charge energy; (b) discharging energy; (c) energy efficiency.

Figure 9 shows the system efficiency calculated using Equation (7). This is inefficient because the energy consumed by the pump increases with the flow rate. Therefore, the system energy required for charging the VRFB stack in Figure 9a can be seen from the fact that more energy is required when the current is small and the flow rate is high. In addition, as can be observed from the discharge system energy in Figure 9b, driving with a high current under low-flow conditions is efficient. This is the effect of the increased pump loss owing to the longer usage time when charging and discharging the battery with a low current, even under low-flow conditions. In the case of the discharge system energy, more energy is required to drive the pump than to supply energy to the load side when used under flow conditions of 350 mL/min or higher (the discharge system energy value is represented as 0). Therefore, the system efficiency in Figure 9c was found to be the highest when the battery was used with a high current (6A) of 200 mL/min.

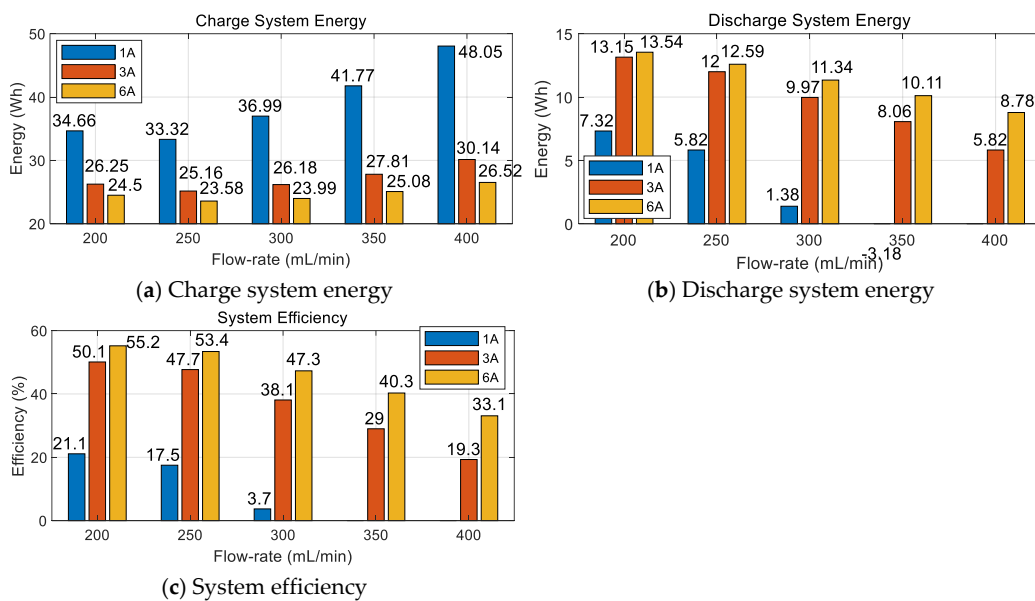


**Figure 9.** VRFB system efficiency under different current and flow conditions: (a) system energy during charging; (b) system energy during discharging; (c) system efficiency.

The VRFB stack system, with cells connected in series, requires optimal operating point analysis to improve efficiency owing to shunt current loss and pump-driving loss. The electrical characteristic test procedure proposed in this study is expected to facilitate rapid and accurate characteristic analysis, aiding in the derivation of an optimal operating method.

### 3.2. Design of Electrical Circuit Model of VRFB

This section presents the electrical circuit model and the parameter design method for the VRFB. In the electrical circuit model (ECM) of the VRFB in Figure 10,  $V_{ocv}$  represents the open-circuit voltage according to the state of charge (SOC), which is the state of charge. The series resistance  $R_i$  and parallel connection circuit of  $R_d/C_d$  in the ECM model were used to simulate the dynamic characteristics of the voltage according to the current. In addition, VRFBs have an internal leakage current called a shunt current, owing to the parallel connection configuration of the electrolyte applied to the series-connected cells. To simulate the shunt current, the ECM has a resistor connected in parallel with the open-circuit voltage [25,26].

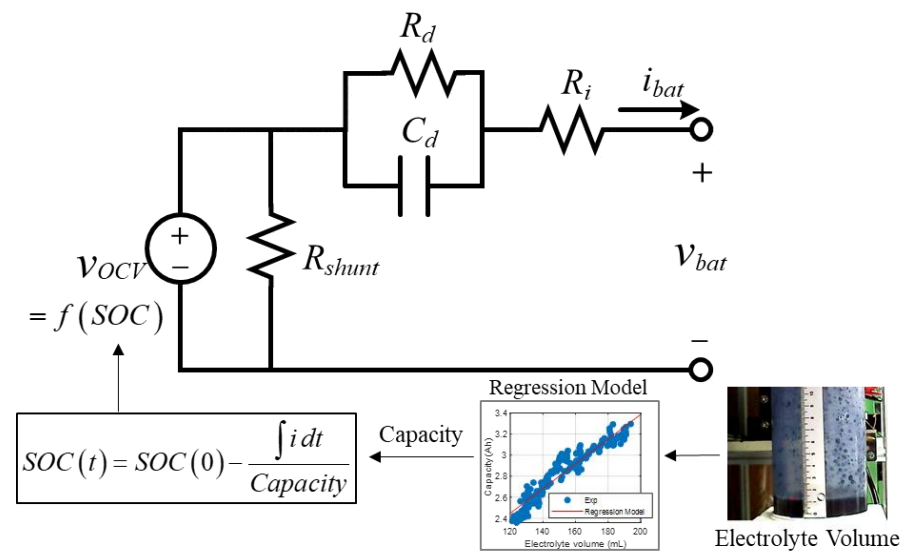


**Figure 10.** Electrical circuit model of VRFB.

The parameters of the open-circuit voltage  $V_{ocv}$  and series resistance  $R_i$ ,  $R_d/C_d$  of the parallel circuit can be obtained by an experiment in which a pulse current is applied to reduce the SOC by approximately 5% from the fully charged state to the fully discharged voltage, as shown in Figure 11, tested using the procedure shown in Figure 4c. The waveform of the period in which the discharge pulse current was applied is shown in Figure 12. The series resistance  $R_i$  is calculated from the voltage drop  $\Delta V$  when a pulse current with a magnitude of  $\Delta I$  is applied using Ohm's law. The parameters of  $R_d$  and  $C_d$  are selected as values that can simulate the voltage relationship of Equation (8), which is obtained by subtracting the magnitude of  $\Delta V$  owing to the series resistance from the battery terminal voltage during times  $t_1$  and  $t_2$  when the current is continuously applied and the change in  $V_{ocv}$  according to the current applied, which is shown in the red waveform in Figure 12. In this study, the  $R_d$  and  $C_d$  parameters were estimated by the least squares method using Matlab software. Figure 13 shows the electrical circuit parameters of the VRFB stack used in this study.

$$R_d i_{bat} \left( 1 - e^{-\frac{t}{R_d C_d}} \right) = v_{bat} - R_i i_{bat} - v_{OCV} \quad (8)$$

To obtain the shunt resistance ( $R_{shunt}$ ) of the electrical circuit model, the pump was driven under no-load conditions and the time to discharge from a fully charged state to a fully discharged voltage was measured for each flow rate. Figure 14 shows the

results obtained when the VRFB stack was used under no-load conditions at a flow rate of 250 mL/min. The measured charge capacity of the battery before the no-load test was 2.89 Ah, and the battery was fully discharged after 39.5 h. Therefore, the VRFB stack can be modeled as having an  $R_{shunt}$  resistance of 76.6  $\Omega$  when operated at 250 mL/min.

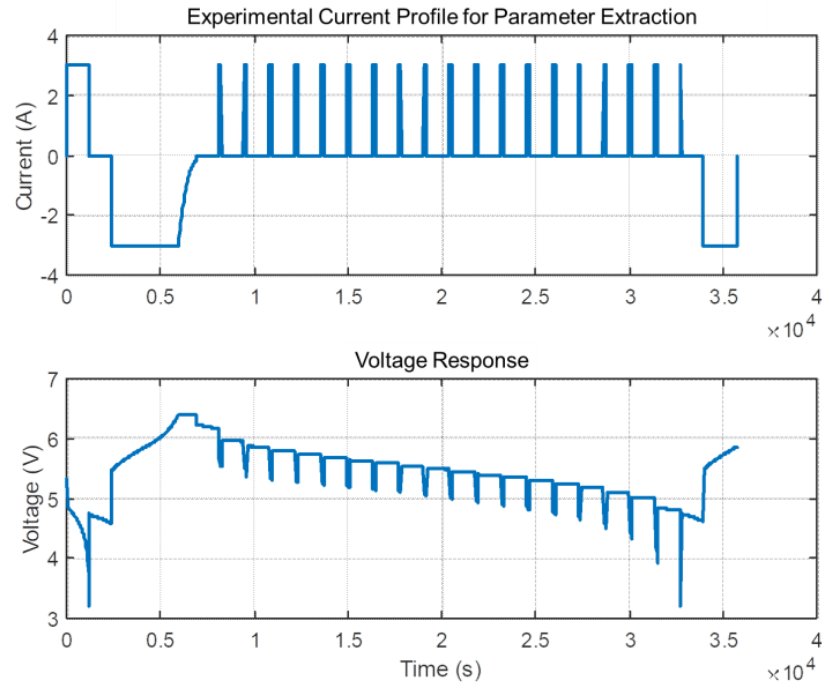


Figure 11. Current and voltage waveforms of experiment for parameter extraction of VRFB.

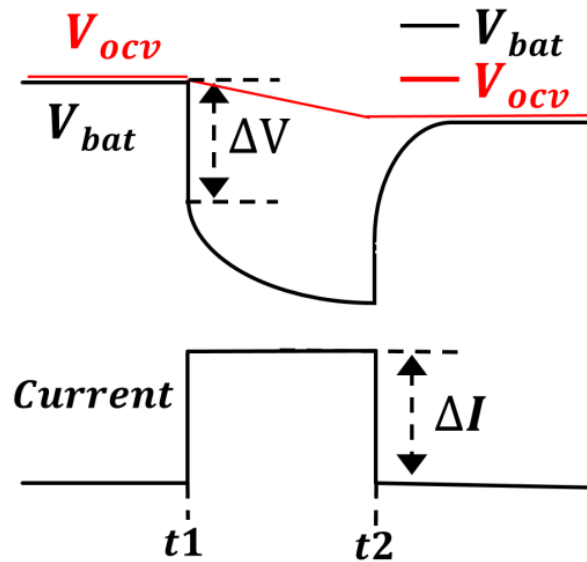


Figure 12. Battery voltage response during pulse current.

The shunt current/resistance values measured under flow rate conditions of 200–400 mL/min using the same test method are listed in Table 3. From Table 3, it can be confirmed that the shunt current increases slightly as the flow rate of the VRFB stack increases. Therefore, in this study, the shunt resistance was modeled as a power series function as a function of the flow rate, as shown in Equation (9).

$$R_{shunt} = -288.6 \times flow\_rate^{4.547} + 76.96 \ (\Omega) \tag{9}$$

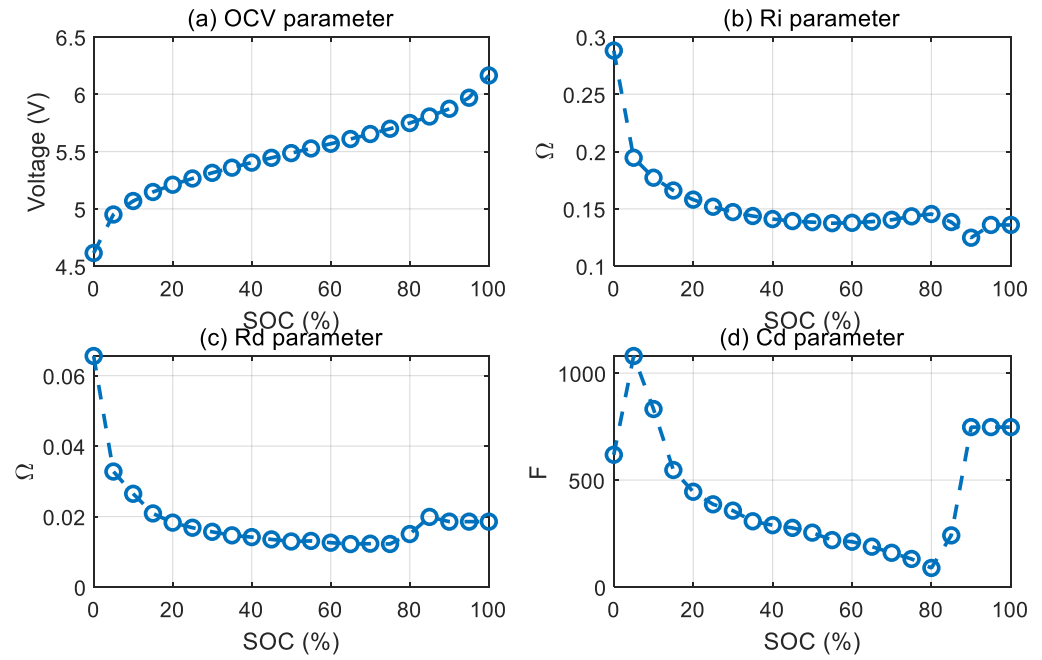


Figure 13. Model parameters of VRFB.

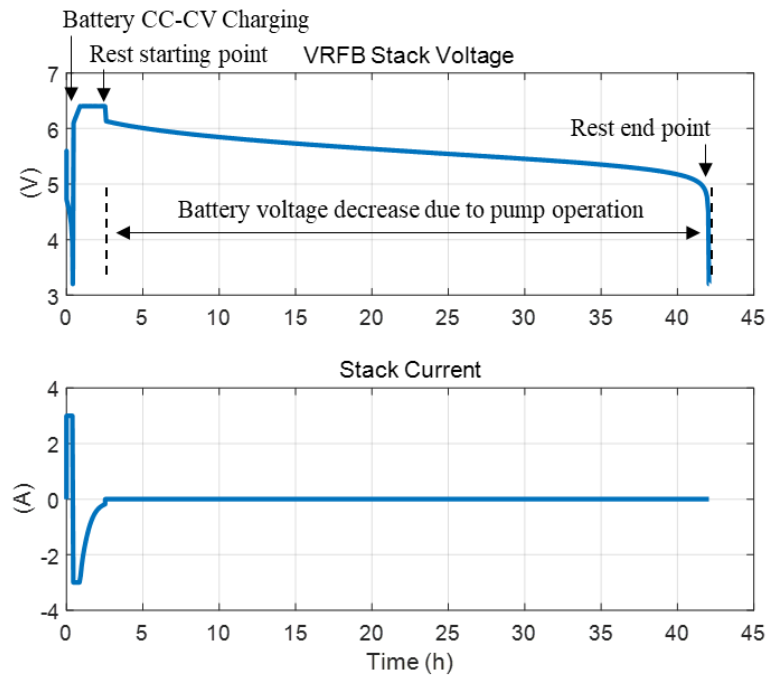


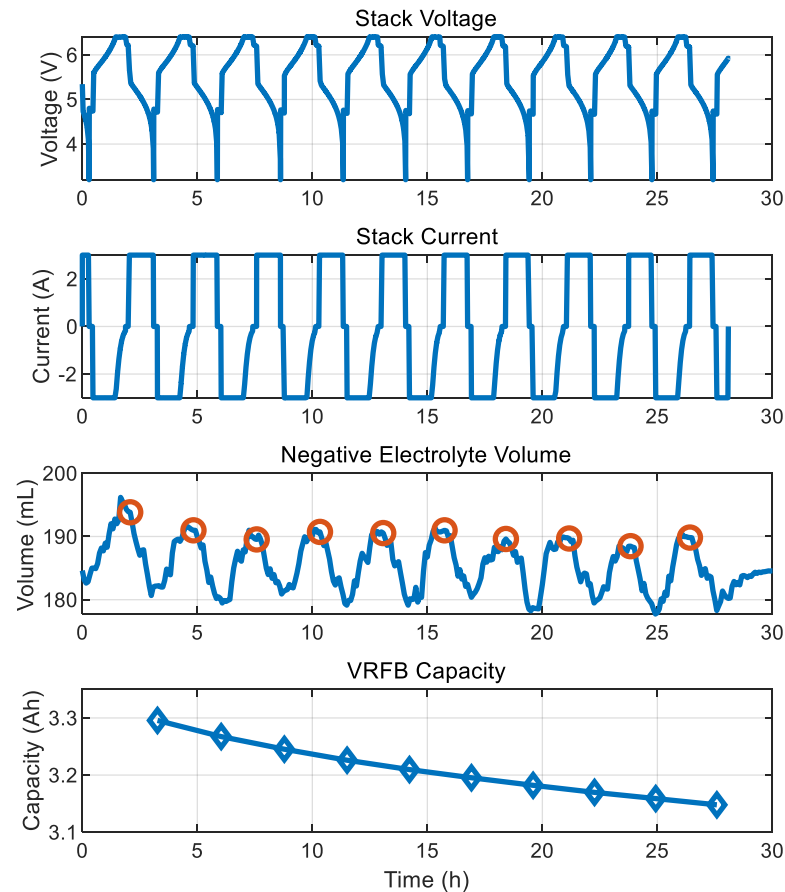
Figure 14. VRFB voltage/current experiment results when the pump is driven at a flow rate of 250 mL/min under no load.

Table 3. Shunt current and resistance by flow rate.

	200 mL/min	250 mL/min	300 mL/min	350 mL/min	400 mL/min
$I_{shunt}$	73.4 mA	73 mA	74.3 mA	75 mA	77.3 mA
$R_{shunt}$	76.7 $\Omega$	76.6 $\Omega$	75.6 $\Omega$	74.6 $\Omega$	72.5 $\Omega$

Figure 15 shows the experimental results of the VRFB cycled ten times under 100% DoD conditions. As shown in the third and fourth waveforms, the volume of the electrolyte

changes during the charging and discharging processes, and the capacity decreases in proportion to the change in the electrolyte. Therefore, in this study, a capacity estimation model for the electrolyte volume was designed and modeled to enable the capacity change by reflecting it in the simulation model.



**Figure 15.** Experimental results of electrolyte volume and capacity change during cycling of VRFB.

The capacity estimation model was designed by analyzing the correlation between the average charge/discharge capacity and negative electrolyte volume in the fully charged state of the battery, which is indicated by the red circle in the third waveform in Figure 15. Figure 16 shows the capacity measurement and estimation results of the linear regression model for the electrolyte volume at 175 fully charged points measured during the long-term cycle of the VRFB battery. For this VRFB system, a capacity estimation model was designed using Equation (10).

$$\text{Capacity} = 0.01173 \times \text{electrolyte volume (mL)} + 1.04 \text{ (Ah)} \quad (10)$$

The validity of the electrically equivalent circuit model of the designed VRFB stack was verified through two charge/discharge experiments. First, as shown in Figure 17a, when the VRFB was used at a flow rate of 250 mL/min, a discharge pulse current of 3 A was applied at approximately every 5% SOC section, and the error between the battery voltage and the simulation model voltage was analyzed. Figure 17b shows the stack voltage measured in the experiment and the simulation model voltage, and the difference between these two voltages is shown in Figure 17c. Except for the fully discharged voltage point with high nonlinearity, the maximum absolute value error of the simulation model is within 0.17 V, and it can be seen that it accurately simulates the actual battery voltage with a root mean square error (RMSE) of 0.025 V.

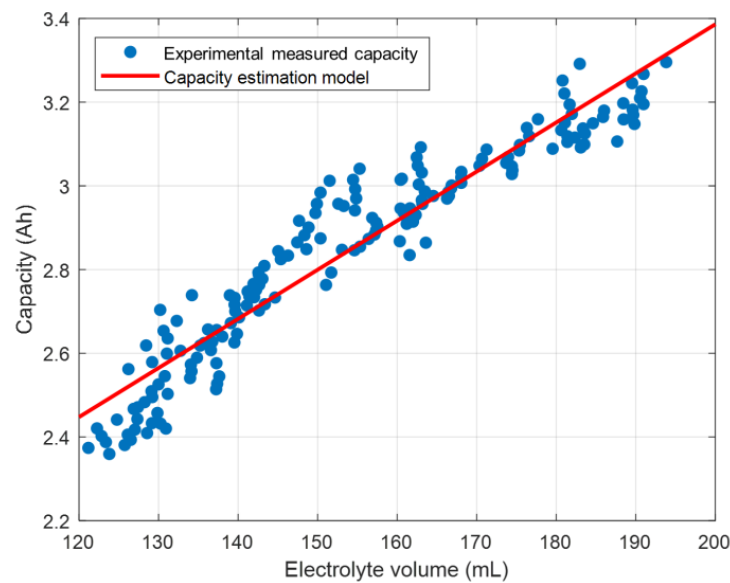


**Figure 16.** Charge/discharge average capacity experimental data and capacity estimation model for 175 electrolyte volumes.

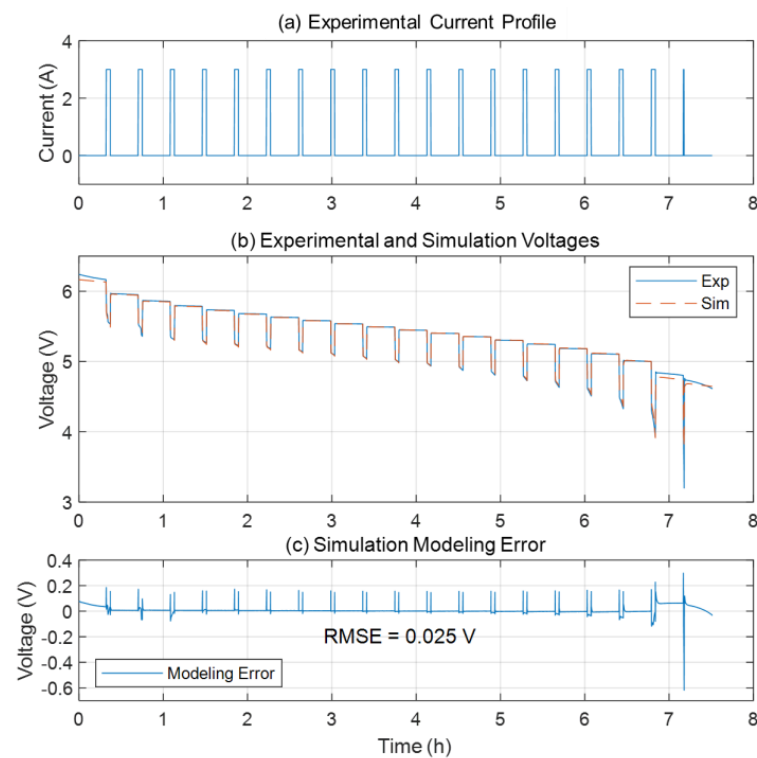


**Figure 17.** Verification of accuracy of a simulation model for discharge pulse current under 250 mL/min: (a) experimental current profile; (b) experimental and simulation voltages; (c) simulation modeling error.

The experimental and modeling simulation results for 11 full charge/discharge cycles with varying currents and electrolyte volumes are shown in Figure 18. The VRFB was fully charged/discharged for the first five cycles with a current of 3 A and then cycled twice, each with currents of 1, 3, and 6 A. Except for a somewhat large voltage error at the full discharge point, it was confirmed that the model could simulate the actual battery voltage within an RMSE of 0.096 V, even when the electrolyte volume and current magnitude were varied.

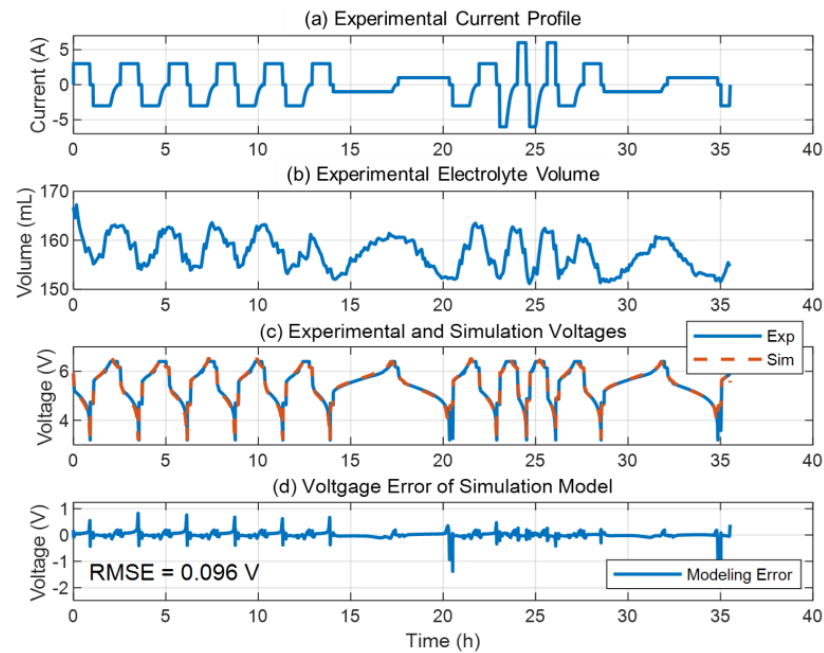


**Figure 18.** Verification of simulation model accuracy when current magnitude and electrolyte volume change under 250 mL/min.

#### 4. Conclusions

In this study, we propose an experimental procedure and analysis method for analyzing the system efficiency of VRFBs according to the current and flow rate conditions and an electrical equivalent circuit modeling design method for simulating VRFBs.

According to the results of the system efficiency analysis, it was confirmed that the VRFB system has a significant impact on the system efficiency owing to the shunt current loss and pump loss for electrolyte transport. For the VRFB system used in this study, it was found that it is efficient to operate a VRFB with a high current under low-flow conditions. In addition, even if the VRFB system is changed, its efficiency characteristics can be quickly analyzed by applying the test and analysis procedures presented in this study.

In addition, this paper presents an electrical circuit modeling and parameter design method that can simulate the electrical output characteristics of VRFBs when the electrolyte volume and flow rate conditions are changed. The proposed simulation model can be used to investigate efficient operational control methods for VRFB systems. The accuracy of the proposed simulation model was verified through comparison with the full charge/discharge cycle experimental results of a 40 W VRFB stack comprising four 10 W cells in series.

**Author Contributions:** Conceptualization, S.L.; Methodology, S.L.; Software, S.L. and H.J.; Validation, Y.-G.S.; Formal Analysis, Y.-G.S.; Investigation, H.J.; Resources, S.L.; Data Curation, H.J.; Writing—Original Draft Preparation, S.L.; Writing—Review and Editing, Y.-G.S.; Visualization, S.L. and H.J.; Supervision, Y.-G.S.; Project Administration, S.L.; Funding Acquisition, S.L. All authors have read and agreed to the published version of the manuscript.

**Funding:** This research was supported by “Regional Innovation Strategy (RIS)” through the National Research Foundation of Korea (NRF) funded by the Ministry of Education (MOE) (2021RIS-002) and a National Research Foundation of Korea (NRF) grant funded by the Korean Government (MSIT) (No. NRF-2021R1F1A1063150).

**Data Availability Statement:** The original contributions presented in the study are included in the article, further inquiries can be directed to the corresponding author.

**Conflicts of Interest:** The authors declare no conflicts of interest.

## References

1. Guney, M.S.; Tepe, Y. Classification and Assessment of Energy Storage Systems. *Renew. Sustain. Energy Rev.* **2017**, *75*, 1187–1197. [[CrossRef](#)]
2. Castillo, A.; Gayme, D.F. Grid-Scale Energy Storage Applications in Renewable Energy Integration: A Survey. *Energy Convers. Manag.* **2014**, *87*, 885–894. [[CrossRef](#)]
3. Shao, Y.; Zhang, H.; Gao, Y.; Jin, B. Dynamic power distribution strategy using multi-objective collaborative optimization for hybrid energy storage systems. *J. Power Electron.* **2023**, *23*, 1517–1528. [[CrossRef](#)]
4. Diaz, L.B.; He, X.; Hu, Z.; Restuccia, F.; Marinescu, M.; Barreras, J.V.; Patel, Y.; Offer, G.; Rein, G. Meta-Review of Fire Safety of Lithium-Ion Batteries: Industry Challenges and Research Contributions. *J. Electrochem. Soc.* **2020**, *167*, 090559. [[CrossRef](#)]
5. Kong, L.; Li, C.; Jiang, J.; Pecht, M.G. Li-Ion Battery Fire Hazards and Safety Strategies. *Energies* **2018**, *11*, 2191. [[CrossRef](#)]
6. Chen, Y.; Kang, Y.; Zhao, Y.; Wang, L.; Liu, J.; Li, Y.; Liang, Z.; He, X.; Li, X.; Tavajohi, N.; et al. A Review of Lithium-Ion Battery Safety Concerns: The Issues, Strategies, and Testing Standards. *J. Energy Chem.* **2021**, *59*, 83–99. [[CrossRef](#)]
7. Cai, T.; Mohtat, P.; Stefanopoulou, A.G.; Siegel, J.B. Li-ion Battery Fault Detection in Large Packs Using Force and Gas Sensors. *IFAC-Pap.* **2020**, *53*, 12491–12496. [[CrossRef](#)]
8. Zhang, R.; Li, X.; Sun, C.; Yang, S.; Tian, Y.; Tian, J. State of Charge and Temperature Joint Estimation Based on Ultrasonic Reflection Waves for Lithium-Ion Battery Applications. *Batteries* **2023**, *9*, 335. [[CrossRef](#)]
9. Mrozik, W.; Rajaeifar, M.A.; Heidrich, O.; Christensen, P. Environmental Impacts, Pollution Sources and Pathways of Spent Lithium-Ion Batteries. *Energy Environ. Sci.* **2021**, *14*, 6099–6121. [[CrossRef](#)]
10. Birkl, C.R.; Roberts, M.R.; McTurk, E.; Bruce, P.G.; Howey, D.A. Degradation Diagnostics for Lithium Ion Cells. *J. Power Sources* **2017**, *341*, 373–386. [[CrossRef](#)]
11. Velázquez-Martínez, O.; Valio, J.; Santasalo-Aarnio, A.; Reuter, M.; Serna-Guerrero, R. A Critical Review of Lithium-Ion Battery Recycling Processes from a Circular Economy Perspective. *Batteries* **2019**, *5*, 68. [[CrossRef](#)]
12. Alotto, P.; Guarnieri, M.; Moro, F. Redox Flow Batteries for the Storage of Renewable Energy: A Review. *Renew. Sustain. Energy Rev.* **2014**, *29*, 325–335. [[CrossRef](#)]
13. Weber, A.Z.; Mench, M.M.; Meyers, J.P.; Ross, P.N.; Gostick, J.T.; Liu, Q. Redox Flow Batteries: A Review. *J. Appl. Electrochem.* **2011**, *41*, 1137–1164. [[CrossRef](#)]
14. Jeong, D.; Jung, S. Numerical Analysis of Cycling Performance of Vanadium Redox Flow Battery. *Int. J. Energy Res.* **2020**, *44*, 5209–5222. [[CrossRef](#)]
15. Bhattarai, A.; Ghimire, P.C.; Whitehead, A.; Schweiss, R.; Scherer, G.G.; Wai, N.; Hng, H.H. Novel Approaches for Solving the Capacity Fade Problem during Operation of a Vanadium Redox Flow Battery. *Batteries* **2018**, *4*, 48. [[CrossRef](#)]
16. Xiong, B.; Zhao, J.; Wei, Z.; Skyllas-Kazacos, M. Extended Kalman Filter Method for State of Charge Estimation of Vanadium Redox Flow Battery Using Thermal-Dependent Electrical Model. *J. Power Sources* **2014**, *262*, 50–61. [[CrossRef](#)]
17. Kim, J.; Park, H. Experimental Analysis of Discharge Characteristics in Vanadium Redox Flow Battery. *Appl. Energy* **2017**, *206*, 451–457. [[CrossRef](#)]
18. Cunha, Á.; Martins, J.; Rodrigues, N.; Brito, F.P. Vanadium Redox Flow Batteries: A Technology Review. *Int. J. Energy Res.* **2015**, *39*, 889–918. [[CrossRef](#)]
19. Jung, H.; Lee, S. A Study on Capacity and State of Charge Estimation of VRFB Systems Using Cumulated Charge and Electrolyte Volume under Rebalancing Conditions. *Energies* **2023**, *16*, 2478. [[CrossRef](#)]
20. Iwakiri, I.; Antunes, T.; Almeida, H.; Sousa, J.P.; Figueira, R.B.; Mendes, A. Redox Flow Batteries: Materials, Design and Prospects. *Energies* **2021**, *14*, 5643. [[CrossRef](#)]
21. Sun, C.; Negro, E.; Nale, A.; Pagot, G.; Vezzù, K.; Zawodzinski, T.A.; Meda, L.; Gambaro, C.; Di Noto, V. An efficient barrier toward vanadium crossover in redox flow batteries: The bilayer [Nafion/(WO<sub>3</sub>)x] hybrid inorganic-organic membrane. *Electrochim. Acta* **2021**, *378*, 138133. [[CrossRef](#)]
22. Kim, S.; Thomsen, E.; Xia, G.; Nie, Z.; Bao, J.; Recknagle, K.; Wang, W.; Viswanathan, V.; Luo, Q.; Wei, X.; et al. 1 Kw/1 Kwh Advanced Vanadium Redox Flow Battery Utilizing Mixed Acid Electrolytes. *J. Power Sources* **2013**, *237*, 300–309. [[CrossRef](#)]
23. Karrech, A.; Regenauer-Lieb, K.; Abbassi, F. Vanadium Flow Batteries at Variable Flow Rates. *J. Energy Storage* **2022**, *45*, 103623. [[CrossRef](#)]
24. Ma, X.; Zhang, H.; Sun, C.; Zou, Y.; Zhang, T. An Optimal Strategy of Electrolyte Flow Rate for Vanadium Redox Flow Battery. *J. Power Sources* **2012**, *203*, 153–158. [[CrossRef](#)]
25. Fornaro, P.; Puleston, T.; Puleston, P.; Serra-Prat, M.; Costa-Castelló, R.; Battaiotto, P. Redox flow battery time-varying parameter estimation based on high-order sliding mode differentiators. *Int. J. Energy Res.* **2022**, *46*, 16576–16592. [[CrossRef](#)]
26. Zhang, Y.; Zhao, J.; Wang, P.; Skyllas-Kazacos, M.; Xiong, B.; Badrinarayanan, R. A comprehensive equivalent circuit model of all-vanadium redox flow battery for power system analysis. *J. Power Sources* **2015**, *290*, 14–24. [[CrossRef](#)]
27. Schwenzler, B.; Zhang, J.; Kim, S.; Li, L.; Liu, J.; Yang, Z. Membrane Development for Vanadium Redox Flow Batteries. *ChemSusChem* **2011**, *4*, 1388–1406. [[CrossRef](#)]
28. Bae, D.; Kanellos, G.; Wedege, K.; Dražević, E.; Bientien, A.; Smith, W.A. Tailored energy level alignment at MoOX/GaP interface for solar-driven redox flow battery application. *J. Chem. Phys.* **2020**, *152*, 124710. [[CrossRef](#)]

29. Jirabovornwisut, T.; Arpornwichanop, A. A review on the electrolyte imbalance in vanadium redox flow batteries. *Int. J. Hydrogen Energy* **2019**, *44*, 24485–24509. [[CrossRef](#)]
30. Chen, S.; Sun, C.; Zhang, H.; Yu, H.; Wang, W. Electrochemical Deposition of Bismuth on Graphite Felt Electrodes: Influence on Negative Half-Cell Reactions in Vanadium Redox Flow Batteries. *Appl. Sci.* **2024**, *14*, 3316. [[CrossRef](#)]

**Disclaimer/Publisher’s Note:** The statements, opinions and data contained in all publications are solely those of the individual author(s) and contributor(s) and not of MDPI and/or the editor(s). MDPI and/or the editor(s) disclaim responsibility for any injury to people or property resulting from any ideas, methods, instructions or products referred to in the content.